GEOPHYSICS®

A case study on receiver-coupling quality assessment from the seismic-interferometry processing of downhole seismic noise recordings

Journal:	*Geophysics*
Manuscript ID	GEO-2018-0293.R2
Manuscript Type:	Case Histories
Keywords:	acquisition, tube wave, interferometry, downhole receivers, microseismic
Area of Expertise:	Seismic Data Acquisition, Passive Seismic and Microseismic Methods
Note: The following files were submitted by the author for peer review, but cannot be converted to PDF. You must view these files (e.g. movies) online.	
table.tex	

A case study on receiver-clamping quality assessment from the seismic-interferometry processing of downhole seismic noise recordings

Sergey Yaskevich [*†], **Anton Duchkov** [†‡], **Artem Myasnikov** [§]

[*] *Novosibirsk State University,*

Pirogova str., b 2 , Novosibirsk, Russia, 630090

[†] *Trofimuk Institute of Petroleum Geology and Geophysics of Siberian Branch Russian Academy of Sciences,*

Koptuga av., b 3, Novosibirsk, Russia, 630090

[‡] *Novosibirsk State Technical University*

Nemirovicha-Danchenko str., b 136, Novosibirsk, Russia, 630087

[§] *Skolkovo Institute of Science and Technology,*

Moskow Russia

(January 23, 2019)

Running head: ***seismic interferometry***

ABSTRACT

ABSTRACT

For downhole microseismic monitoring of hydraulic fracturing, the acquisition is performed using a set of 3C seismic receivers attached firmly to the borehole wall by a clamping mechanism. Such an acquisition cannot be repeated and it is focused on recording weak signals. Thus, proper installation of the receivers is especially crucial for microseismic applications. Here, we present a case study of using a seismic-interferometry approach for assessing the receiver's installation quality from ambient-noise records. Crosscorrelation of one vertical receiver noise records with the others allows us to retrieve the direct body wave propagating along the receiver array. Our observations show that the inability to retrieve the direct body wave is an indicator of clamping issues. Our case study does not support the *emergence frequency* hypothesis reported in the literature (that higher frequencies present in the retrieved body-wave spectrum imply better clamping quality). Another conclusion is that the seismic-interferometry processing provides a stable assessment of the clamping quality only for the vertical receivers. Thus, one gets only partial diagnostics of the clamping quality for the 3C downhole tool. This is important because the horizontal components may be affected more by the clamping issues compared to the vertical components. The overall conclusion is that seismic-interferometry processing of noise records is recommended for the assessment of the downhole receiver installation prior to microseismic monitoring. It does not provide complete diagnostics but comes for free (does not need any additional technological operations or extra time).

INTRODUCTION

Microseismic monitoring is an actively used technology in modern oil and gas exploration. It partially follows the traditional seismological ideas, where instead of using controlled sources, induced earthquakes are observed. The seismic recordings are used for localising microseismic events and updating medium parameters (Grechka and Yaskevich, 2014). For data acquisition, seismic receivers are placed deep in the borehole (Maxwell et al., 2010a) or at the surface (Duncan and Eisner, 2010). In this paper, we focus on downhole data acquisition, when 3-component (3C) seismic receivers are located close to the process of interest (for example hydraulic fracturing). A representative number of microseismic events can be observed in this case due to the small distance between event hypocenters and the monitoring well (Rutledge and Phillips, 2003).

Downhole seismic receivers are placed in a relatively quiet place that in general provides one with a high signal-to-noise ratio (SNR). Usually, for borehole data it is possible to observe P- and S- waves and to determine their arrival times. The amplitude of the recorded signal mostly depends on the magnitude of the event, the distance from its hypocenter, and the quality of the receiver coupling with the medium. The properties of the seismic receiver placement in the borehole are carefully studied in the practice of vertical seismic profiling (VSP) (Hardage, 1981; Van Sandt and Levin, 1963; Galperin, 1974). The seismic tools used for microseismic monitoring are similar to those used in VSP or sometimes just the same. Thus, we will revisit main VSP findings taking into account the special features of microseismic monitoring: in particular the much longer acquisition time, and the wider frequecy band of interest (15 to 500 Hz).

Placement of a seismic 3C receiver into a well needs a special clamping mechanism to attach the tool firmly to the borehole wall. The most popular clamping mechanism is a steel arm (clamping force is controlled by electric power). This mechanical attachment of the downhole seismic tool (as well as any other mechanism) forms a damped oscillatory system which was shown both theoretically (Lamer, 1970; Beydoun, 1984) and practically (Wuenschel, 1976; Gaiser et al., 1988). Due to the cylindrical tool form, the oscillatory properties are different in the transverse and aligned with borehole direction (Gaiser et al., 1988). Wuenschel (1976) shows the influence of coupling mechanics on the response of the vertical component (aligned with the axis of the tool) using internal shakers. They discuss two experimental setups: the tool is clamped and when the same tool is not clamped. Wuenschel (1976) also shows that the tool with bad clamping has a strong oscillatory resonance around 50 Hz, which is within the seismic band of interest for VSP studies and that reasonable clamping moves this resonance above 500 Hz. This is enough for VSP as well as for microseismic studies. Gaiser et al. (1988) show that for the quality control in VSP studies it is extremely important to pay more attention to the resonances on the horizontal components. They find these resonances to occur at 80 and 130 Hz depending on the tool construction including the: size of the clamping arm, the clamping force and the area of tool-borehole contact. Note that the resonance at 130 Hz might be acceptable for VSP but it is still within the frequency range of interest for microseismic monitoring. Despite continuing progress in downhole seismic tools, one can still observe resonances caused by clamping issues in the raw microseismic monitoring data (Zhang et al., 2016). Such resonances are observed in microseismic event records and their spectra. In the seismic record, a resonance shows up as a continuous oscillation (20 ms and longer) after the direct body-wave arrival (we will use the term “ringing effect” in the paper to name this phenomenon). In the spectra, this resonance causes spikes at a certain resonant frequency. In the paper, we treat the presence of such a phenomenon as a proof of poor clamping which directly leads to poor coupling. There is also a known tool adjustment - installation of the internal shakers into the tool which provides one with direct clamping-quality control (Montmollin, 1988), but this method is seldom applied in modern tools.

In addition to the discussed resonances, placement of a seismic tool in a cemented borehole, filled with fluid results in characteristic seismic noise. The level of this noise may vary from place to place and may change during the monitoring itself (Maxwell et al., 2006). Understanding the nature of this noise is important as the processing results may be ambiguous and cause false interpretation as a result of low SNR (Maxwell et al., 2010b). This noise includes coherent and random components. Coherent noise is formed by all body waves travelling from the different directions and tube waves propagating mostly in the fluid column. The upper part of the fluid column is exposed to interactions with surface waves (ground roll) which hit the wellhead and act as the main source of tube waves. After their initiation, tube waves show very small attenuation in the fluid column. In order to reduce tube-wave energy, the fluid level is lowered to weaken the interaction of the borehole fluid with the surface waves. The receiver design is also aimed to lower their energy in the recordings. In VSP data, the tube waves appear after the arrival of the downgoing direct body wave and distort the phases of the reflected waves. In microseismic monitoring, the tube waves may show up as a clear arrival or may be weaker and hidden in the background noise. In the second case, they reduce the quality of the data, making the determination of wave arrivals more ambiguous. In a perfectly cemented well, the amplitudes of the recorded tube waves in the seismic record decrease dramatically with increasing clamping force (Van Sandt and Levin, 1963). The other quality which influences the energy of the tube waves is the quality of borehole wall cementing. In case of bad cement, the tube waves will not attenuate on the wall (Hardage, 1981) and reduce the record quality. In this case, better clamping will not reduce the tube wave energy as the borehole casing is shaking with the tube wave.

The downhole microseismic monitoring generally relies on signals which are usually much weaker than in the VSP acquisition. After receiver installation data are recorded for much longer periods of time, without any possibility to repeat the acquisition in case of a poor record. For microseismic monitoring, the issues with the quality of the receivers coupling are of great importance. Thus, the industry is in need of methods to assess the quality of each particular tool installation.

Here, we revisit the seismic-interferometry processing, which is based on cross-correlation of noise records of two receivers resulting in the virtual-source gather (Bakulin and Calvert, 2006) as if one of the receivers acted as a source and the another as a receiver (Claerbout, 1968; Wapenaar et al., 2010; Schuster, 2016). For shallow downhole microseismic monitoring ($<$ 700 m depth), Miyazawa et al. (2008) show that month-long noise recordings may be used to reconstruct downgoing direct P- waves, using the vertical component of the record, and S- waves using the horizontal components of the record. For a deeper acquisition ($\approx$ 3000 m) the vertical component may be used to reconstruct the direct P- wave (Grechka and Zhao, 2012), which is shown for several datasets and much shorter total record time (5 minutes). Vaezi and Van der Baan (2015) show that tube waves can also be retrieved with seismic interferometry, and suggest that their dominance in a wide frequency range reveals tool-clamping problems. Vaezi and Van der Baan (2015) also provide a wider variety of examples and propose an approach to assess the clamping quality of the receiver based on the proposed term - *emergence frequency*, which means " the frequency below which direct body waves propagating along the receivers are observed on the crosscorrelation gathers".

The suggestion was that if this frequency is about 15-20 Hz it is a sign of poorer coupling, the frequency of 60 Hz was suggested to be a sign of the better clamping of the receiver. Note that the vertical component is used for the proposed suggestions; the authors did not retrieve body waves on the horizontal components of the record.

Here, we apply this seismic-interferometry based processing to several downhole microseismic monitoring datasets. All datasets were acquired with similar equipment at similar depth but show different issues with the tool installation, instead of the different acquisitions in Vaezi and Van der Baan (2015). In addition to previous results, we present seismic record examples showing coupling-related recorded resonances, justifying some aspects of the methodology. Finally, we present our conclusions on the effectiveness of seismic interferometry for assessing downhole seismic-tool placement prior to hydraulic fracturing, and on the *emergence frequency* hypothesis.

METHOD DESCRIPTION

In our paper, we follow the processing of downhole microseismic-noise record described in Vaezi and Van der Baan (2015) and the general original approach was described in Bensen et al. (2007). The workflow is designed to be applied to the same components of 3C downhole seismic receivers record. Because of the tool form, the vertical component of the 3C receiver is directed along the borehole and the other two components are orthogonal to the borehole direction and to each other (other options are possible (Plotnitskii et al., 2018)).

For each component of the noise record, the following processing steps are to be applied:

1. Remove the trend and apply instrument correction if needed (in case of different sensors, the record of the geophone with a broader bandwidth should be corrected to

the frequency range of narrower band geophone) (Bensen et al., 2007).

2. Apply 1-bit normalisation in the time domain to reduce the influence of non-stationary sources of noise (replace the observed amplitudes with their sign) (Larose et al., 2004). This means that the resultant trace contains only the strongest arrival at each time sample.

3. Apply spectral whitening to increase the resulting crosscorrelation function's bandwidth and prevent spectral peaks from overwhelming the crosscorrelation functions (the signal spectrum is normalised to its smoothed version) (Bensen et al., 2007).

As a result, we get a set of continuous records $a_r(t)$, index r denotes a seismic receiver. The rest of the seismic-interferometry processing consists of the following steps:

1. Divide a long noise record into 5- to 10-second-long gathers $a_r^j(t)$, $j = 1, ..., N$, where N is the number of time intervals.

2. Select a reference geophone $a_{ref}^j(t)$, which acts as a virtual source for the rest of the analysis.

3. Cross-correlate the record of the reference with other receivers, then we sum over the N time intervals:

$$A_{r_{ref},r}(\tau) = \sum_{j=1}^{N} \sum_{t} a_{r_{ref}}^j(t) a_r^j(t+\tau), \qquad (1)$$

where τ is the displacement, also known as lag. The result of this crosscorrelation is usually called a virtual-source gather (Bakulin and Calvert, 2006).

4. Apply different band-pass filters to the virtual-source gather and normalise traces. We characterise band-pass filters by their corner frequencies [f1-f2-f3-f4] Hz.

5. Steps 2-4 are repeated for different reference geophones if any of the observed waves vanishes at some receiver.

The resultant virtual-source gathers usually contain only direct body or tube waves. Different band-pass filters are then used to analyse the frequency range of the body wave in more details. The *emergence frequency* hypothesis from (Vaezi and Van der Baan, 2015) suggests that the lower frequencies of low pass filter we need to achieve clear body waves in the virtual-source gather the worse is the receiver clamping quality.

DATA EXAMPLES

Here, we apply the described method to four downhole microseismic-monitoring datasets A, B, C, and D, collected to monitor hydraulic fracturing in a tight formation. The fracturing goal was effective hydro-carbonates production. The schematic acquisition geometry for these datasets is shown in Figure 1. All acquisitions were made at a depth of ≈ 2000-3000 m with almost the same tools: same clamping mechanism, same tool/borehole diameters relationship, in all datasets 15-Hz geophones were used, the sampling rate was the same - 4000 Hz, monitoring wells were almost vertical, the acquisitions are almost of the same length and nearly the same number of geophones were used (dataset D includes 7 geophones instead of 8). In all cases, we process the record with seismic interferometry using 5-minute long record made prior to hydraulic fracturing. Because (Vaezi and Van der Baan, 2015) show that the method is effective for the vertical-receiver coupling assessment - we here also primarily consider the vertical component for all datasets. We selected these datasets based on the criteria that the acquisition geometry is similar but with different interferometry application results.

[Figure 1 about here.]

For dataset A in Figure 2, we show the virtual-source gathers (for the vertical component, the first receiver is the virtual source). The applied band-pass filter parameters are: [5-10-500-2000] Hz (Figure 2, a), and [5-10-30-60] Hz (Figure 2, b). The first virtual-source gather in Figure 2, a) is dominated by the down-going and up-going tube waves with an apparent velocity of about 1.5 km/s (shown with a dotted line). The up-going wave is the tube wave reflected from the packer installed below the acquisition array (the up-going wave is shown with a dotted line). For the narrower band-pass filter (corner frequencies [5-10-30-60] Hz) the resulting virtual-source gather is dominated by the direct body wave with a much higher velocity (3,5 km/s), which is close to the P-wave velocity from the acoustic log data. The quality of the direct body wave degrades with distance between the virtual-source and the receiver. We suggest that the loss of direct body wave energy is caused by increased noise level for this dataset. The virtual-source gathers computed for the fourth receiver as virtual source show stable direct body wave amplitude (see Figure 2 c),d)), suggesting a uniform clamping condition.

In this dataset (A), only a few microseismic events are observed – insufficient to make clear conclusions about the hydraulic-fracture geometry (Yaskevich et al., 2015). A record of one of the microseismic events is shown in Figure 3 (filtered with a band-pass [40-50-200-400] filter). We do not see typical ringing effects (corresponding to clamping-related oscillations) in this record or in any other record in this dataset. At the same time, this dataset is characterised by an extremely high noise level and a large number of intensive tube waves observable in the raw recordings (because fluid level was not lowered in the monitoring well we think this also resulted in the background noise enhancement). Fracturing itself was comparatively distant – about 500 m from the monitoring well. We think that two factors have resulted in a low S/N ratio in microseismic events records in this case. First, the acquisition was too distant from the fracturing area. Second, the high energy of the background noise.

[Figure 2 about here.]

[Figure 3 about here.]

In Figure 4, we show the virtual-source gathers for dataset B (we use the vertical component, the first receiver as a virtual source), band-pass-filter parameters are [5-10-500-2000] Hz (Figure 4, a) and [5-10-30-60] Hz (Figure 4, b). Both gathers are dominated by a direct body wave with higher apparent velocity (about 4.0 km/s). We do not observe any tube wave on the resulting virtual-source gathers for any frequency. Unlike dataset A, the resulting body wave energy does not vary along the receivers line.

In dataset B, the distance from the observation well to the fracturing area was much shorter (250 - 300 m). A lot of microseismic events are observed. We observe no "ringing" in the microseismic event records. The fluid level in the monitoring well was lowered to 400 m below the wellhead. From the microseismic event-record quality we qualify this dataset as being well and uniformly clamped and coupled with the medium.

[Figure 4 about here.]

For dataset C, we show virtual-source gathers in Figure 5. We filter them with a band-pass filter [5-10-500-2000] Hz (a), and [5-10-30-60] Hz (b) - with the first receiver as a virtual source. Both gathers are dominated by the direct body wave with an apparent velocity of about 4.0 km/s (close to the P- wave velocity in the media) except for the 8th receiver where the body-wave phase vanishes. Panels c) and d) show virtual-source gather for the 8th receiver as a virtual source. In Figure 5, c) we apply a band-pass filter [5-10-30-60] Hz and observe the downgoing tube wave instead of the body wave. Then we applied several band-pass filters trying to retrieve the body wave, but were not able to recover a body wave. At the lower frequencies, when the virtual-source gather is filtered with a [1-5-10-20] Hz band-pass filter, the tube wave disappears as shown in Figure 5, d) and there is no clear sign of the body wave. Summarising the approach results for this dataset, seismic interferometry clearly shows a problem with clamping for the 8th receiver. Other receivers are uniformly clamped.

In terms of the microseismic event records, dataset C looks different from dataset B, we observe many fewer events in the data, despite the fact that all acquisition parameters were similar (same geology, similar tools, and noise sources on the surface). We show an example of a microseismic event in Figure 6. For the 8th receiver, we clearly see the "ringing" on the vertical component – this is the long oscillation envelope following the direct-wave arrival (the frequency is about 280 Hz), weaker but still recognisable effects are observable for the horizontal components. This is a clear indication of clamping problems for the 8th receiver.

[Figure 5 about here.]

[Figure 6 about here.]

For the last dataset, D, seismic-interferometry results are shown in the Figure 7 (we use the vertical component , with the first receiver as a virtual source). The band-pass filter parameters are [5-10-500-2000] Hz (Figure 7, a) and [5-10-30-60] Hz (Figure 7, b). Both gathers are dominated by body wave arrivals with a dominant frequency of 50 Hz. In this case, seismic interferometry suggests good (high *emergence frequency*) and uniform clamping.

[Figure 7 about here.]

[Figure 8 about here.]

[Figure 9 about here.]

The example of microseismic event recording for dataset D is shown in Figure 8 (for receivers 5, 6, and 7). We see the clear "ringing" oscillations for receivers 5 and 6 (horizontal receivers), the resonant nature of this phenomenon is observed in Figure 9. Hundreds of events were detected during monitoring but the recording quality was poor: the horizontal-component resonant oscillations start with the P- wave arrival and overlap the subsequent S-wave arrival. This makes it problematic to determine the S- wave arrival-times and harmes the quality of the polarisation analysis. There is a difference between resonances observed in datasets D and C: for the previous dataset C, we observed severe "ringing" on all components of the 8th receiver. In dataset D, we observe "ringing" mostly on the horizontal components of receivers 1, 4, 5, and 6. The frequency of these oscillations is about 130-140 Hz which is similar to the examples from Gaiser et al. (1988) showing records affected by resonances in the horizontal receivers.

In the presented data examples the clear observation is that the produced virtual-source gathers are mostly one-sided, which happens when the seismic noise sources are not distributed homogeneously (Shapiro and Campillo, 2004). For the studied datasets, we suggest that the seismic noise is anthropogenic and propagates from surface facilities. The absence of other waves in the crosscorrelation gathers may be caused by several fators, two of which are major: low energy level of the waves (below the electric noise of the recording system) and the processing workflow. The later may be addressed with more accurate signal normalization (Draganov et al., 2013) instead of 1-bit. For the studied datasets, we are quite certain about the absence of bursts, because not using 1-bit normalisation did not change the quality of the crosscorrelation results significantly, which indicates that we do not miss a lot with the data processing. If other arrivals are of the interest we will need to consider longer records.

DISCUSSION

Summary of the data examples

In the paper, we analysed several real microseismic datasets following seismic-interferometry processing suggested by (Vaezi and Van der Baan, 2015) to check the clamping quality of borehole receivers. For all datasets from that paper, the tube and body waves are both retrieved in the virtual-source gathers. Thus, band-pass filtering is necessary to identify the body-wave *emergence frequency* as otherwise it is masked by the tube waves. We retrieve a visible tube waves only for datasets A and C, and we do not retrieve it for datasets B and D. In other works, tube waves are also not always retrieved in the virtual-source gathers (Grechka and Zhao, 2012). This leads us to the discussion - how to determine the *emergence frequency* in such a case. It either may me be determined as ∞ - because no filtering is needed to retrieve clear body wave phase, or it may be treated as highest frequency in the retrieved body wave phase - the frequency at which the retrieved body wave emerges. We think that the second definition is more correct and we will use it further. Note that band-pass filtering is not so crucial when there are only body waves in the virtual-source gathers. We can analyse the Fourier spectrum of the retrieved body wave in virtual-source gather to identify the *emergence frequency*, i.e., the highest frequency of the emerged body wave (in the band of interest 10-150 Hz). We show examples of the Fourier spectra for the virtual-source gathers from different datasets in Figure 10 to justify the estimated *emergence frequencies*. For dataset A only adjacent to the virtual source receivers (2-4) are considered for the *emergence frequency* estimate, which is about 30 Hz , for other receivers the spectra are flat, and not useful for the assessment (this is caused by body wave degradation, mentioned earlier). For datasets B, C spectra look similar to each other and the *emergence frequency* estimates are 30 Hz for both datasets, except for the 8th receiver of dataset C, where the higher frequencies of the amplitude spectrum are formed by the retrieved tube wave and no body wave energy is retrieved at any frequency range. For the dataset D the *emergence frequency* assessment is about 50 Hz. The same assessment my be done by the retrieved body wave wavelength analysis on the virtual source gathers.

We summarise the main characteristics of the datasets in Table 1 (the *emergence frequency* and predicted clamping quality, clamping quality assessed from the raw data using visual analysis, spectral characteristics of the retrieved body waves, number of recorded events). We assume that the clamping quality for dataset A is worse than for datasets B, C because of the body-wave degradation from the upper receiver down, see Figure 10, A. On the other hand, we do not see clear clamping issues in the microseismic records. The 8th receiver of dataset C is poorly clamped: the body wave is not retrieved in the virtual-source gathers and coupling-related resonances are observed in the microseismic data. For dataset D, the clamping quality was evaluated as the best one which is consistent with the highest *emergence frequency* observed. We discuss the emergence-frequency results further in this section.

Orientation-shot spectra

In this subsection, we analyse the frequency content of the orientation shots. The orientation shots are made after the borehole tool placement in order to determine the orientation of the receiver components. For all datasets, impulsive sources at the surface were used for the orientation (exact source parameters are unknown, but they should be similar for all studied datasets). The spectra of the orientation-shot records are shown in Figure 11 for the selected traces from all four datasets. The main observation here is that the signal from dataset D contains higher frequencies compared to datasets A, B, and C. This may be attributed to the less-attenuating geologic section and the shallower depth of acquisition for dataset D which can also explain the higher-frequency content in the spectra of the virtual-source gathers (see Figure 10). The higher number of the observed events (Table 1) is mostly related to the less distant acquisition and probably higher seismogenic index (Shapiro et al., 2010).

Another important observation is that the orientation-shot records do not show problems with the clamping quality. Even for the worst case of clamped problems (8th receiver in dataset C) the orientation-shot spectra appear similar to other ones. Thus, the orientation-shot records are not very useful in revealing problems with the clamping quality. Most likely, they just do not contain higher frequencies which may be close to the clamping-related resonances (150-300 Hz).

Emergence-frequency discussion

Various factors may result in different frequency content of the direct body wave in the downhole virtual-source gathers. In particular, we think that the source frequency content and the rock attenuation properties may be important factors affecting the frequency content of the retrieved body waves in the virtual-source gathers. These factors may vary from site to site and thus may not be in agreement with the hypothesis from (Vaezi and Van der Baan, 2015) that lower *emergence frequency* means worse clamping quality. Moreover, note that considering the differences in the *emergence frequency* of 10 and 30 Hz we are talking about signal wavelengths of 300 and 100 m, respectively correspondingly. Both wavelengths are much longer than the longest tool dimension (2 m).

The clamping mechanism provides an attachment of the 3C seismic tool to a borehole wall. Although the horizontal components may have lower clamping quality compared to the vertical component, they still should be correlated for the same tool: better coupling quality of the vertical component means overall better coupling quality for the horizontal components. In our case study, we have controversial observations while comparing dataset D to the other datasets. It should have the best coupling quality for the vertical component if derived from the highest *emergence frequency* (50 Hz compared to 30 Hz for the other datasets). At the same time, the horizontal-component records show stronger resonances indicating that the coupling problems are worse for this dataset compared to the others. Thus, we suggest that the *emergence-frequency* differences between the datasets are not related to the clamping quality but rather may depend on the attenuation properties of the rocks at the particular site.

Horizontal-component crosscorrelation

Seismic interferometry applied to short (5-15 minutes) horizontal-component records did not result in a clear waves retrieval for any of the datasets considered. Similarly, seismic-interferometry processing was reported mostly for vertical components in other papers. We know only one paper reporting reconstruction of shear waves from noise records (Miyazawa et al., 2008), which required a month-long noise recording and shallow receiver placement ($\approx$ 700 m). In that paper, the authors explained the one-sided shape of the virtual-source gathers by high attenuation of the shear waves. The same explanation was used by Vaezi and Van der Baan (2015) to explain the absence of shear waves after the crosscorrelation of horizontal components. So, it seems that the shear waves are too attenuated at the depth of 2-3 km to be retrieved by seismic interferometry of microseismic records.

[Figure 10 about here.]

[Figure 11 about here.]

CONCLUSIONS

Downhole seismic data acquisition for microseismic monitoring requires seismic receivers to be coupled with media perfectly to record weak signals with good quality. In our paper, we followed the reported idea of seismic-interferometry processing of noise records in order to assess the coupling quality of downhole receivers. We show the results of virtual-source gather retrieval for several real microseismic-monitoring datasets. For our datasets, we compare the results of the seismic-interferometry processing with the analysis of the microseismic-monitoring dataset itself. From our case study, we make the following conclusions:

1 Our results partially confirm previous observations that strong tube waves in the virtual-source gathers and reduced energy of the retrieved body waves indicate that there are problems with the downhole-tool coupling.

2 We do not see unambiguous confirmation of the hypothesis that a higher *emergence frequency* indicates better coupling quality. For our datasets, the increase of the *emergence frequency* (from 30 to 50 Hz) is not directly correlated with the enhancement of the microseismic-record quality.

3 We suggest that seismic-interferometry processing preceding microseismic monitoring may help in revealing problems with the downhole- tool coupling while not requiring any additional acquisition effort. One can assess the vertical-component coupling so that the tool can be re-installed before microseismic monitoring begins.

The suggested clamping-quality assessment is not complete for the 3-component tool, especially when keeping in mind that the horizontal components are more sensitive to clamping issues. In view of mentioned limitations, it worth revisiting the idea of installing shakers into the borehole seismic tools for direct control of clamping quality. This idea was discussed in 80–90s for VSP instruments; it is, though, implemented only in a few tools.

ACKNOWLEDGMENTS

The work was partially supported by RFBR grant N 16-35-60087. We also would like to thank three anonymous reviewers and the associate editors (Dr. Deyan Draganov and Dr. Alison Malkolm) for helpful corrections.

REFERENCES

Bakulin, A., and R. Calvert, 2006, The virtual source method: Theory and case study: GEOPHYSICS, **71**, SI139–SI150.

Bensen, G., M. Ritzwoller, M. Barmin, A. Levshin, F. Lin, M. Moschetti, N. Shapiro, and Y. Yang, 2007, Processing seismic ambient noise data to obtain reliable broad-band surface wave dispersion measurements: Geophysical Journal International, **169**, 1239–1260.

Beydoun, W., 1984, Seismic tool-formation coupling in boreholes: Vertical Seismic Profiling part B: Advanced Concepts: Geophysical press, 80–86.

Claerbout, J. F., 1968, Synthesis of a layered medium from its acoustic transmission response: GEOPHYSICS, **33**, 264–269.

Draganov, D., X. Campman, J. Thorbecke, A. Verdel, and K. Wapenaar, 2013, Seismic exploration-scale velocities and structure from ambient seismic noise (> 1 hz): Journal of Geophysical Research: Solid Earth, **118**, 4345–4360.

Duncan, P., and L. Eisner, 2010, Reservoir characterization using surface microseismic monitoring: GEOPHYSICS, **75**, 139–146.

Gaiser, J. E., T. J. Fulp, S. G. Petermann, and G. M. Karner, 1988, Vertical seismic profile sonde coupling: GEOPHYSICS, **53**, 206–214.

Galperin, E., 1974, Vertical seismic profiling: Society of exploration geophysicists, Tulsa.

Grechka, V., and S. Yaskevich, 2014, Azimuthal anisotropy in microseismic monitoring: A bakken case study: GEOPHYSICS, **79**, KS1–KS12.

Grechka, V., and Y. Zhao, 2012, Microseismic interferometry: The Leading Edge, **31**, 1478–1483.

Hardage, B., 1981, An examination of tube wave noise in vertical seismic profiling data: GEOPHYSICS, **46**, 892–903.

Lamer, A., 1970, Couplage sol-geophone: Geophysical Prospecting, **18**, 300–319.

Larose, E., A. Derode, M. Campillo, and M. Fink, 2004, Imaging from one-bit correlations of wideband diffuse wave fields: Journal of Applied Physics, **95**, 8393–8399.

Maxwell, S., U. Zimmer, N. Warpinski, and C. Waltman, 2006, Quality control/assurance reporting of passive microseismic data, *in* SEG Technical Program Expanded Abstracts 2006: Society of Exploration Geophysicists, 1585–1589.

Maxwell, S. C., J. Rutledge, R. Jones, and M. Fehler, 2010a, Petroleum reservoir characterization using downhole microseismic monitoring: GEOPHYSICS, **75**, 75A129–75A137.

Maxwell, S. C., W. B. Underhill, L. Bennett, C. Woerpel, A. Martinez, et al., 2010b, Key criteria for a successful microseismic project: SPE Annual Technical Conference and Exhibition, Society of Petroleum Engineers, SPE 134695.

Miyazawa, M., R. Snieder, and A. Venkataraman, 2008, Application of seismic interferometry to extract p-and s-wave propagation and observation of shear-wave splitting from noise data at cold lake, alberta, canada: GEOPHYSICS, **73**, D35–D40.

Montmollin, V., 1988, Shaker tests on downhole seismic tools: GEOPHYSICS, **53**, 1160–1168.

Plotnitskii, P., S. Yaskevich, and A. Duchkov, 2018, Using four-component geophones: Effect on the quality and reliability of multicomponent seismic recording and analysis of processing methods: Seismic Instruments, **54**, 401–407.

Rutledge, J. T., and W. S. Phillips, 2003, Hydraulic stimulation of natural fractures as revealed by induced microearthquakes, carthage cotton valley gas field, east texas: GEOPHYSICS, **68**, 441–452.

Schuster, G. T., 2016, *in* Encyclopedia of Exploration Geophysics 5. Seismic Interferometry: Society of Exploration Geophysicists, Q1–1–Q1–41.

Shapiro, N. M., and M. Campillo, 2004, Emergence of broadband rayleigh waves from correlations of the ambient seismic noise: Geophysical Research Letters, **31**, L07614.

Shapiro, S. A., C. Dinske, C. Langenbruch, and F. Wenzel, 2010, Seismogenic index and magnitude probability of earthquakes induced during reservoir fluid stimulations: The Leading Edge, **29**, 304–309.

Vaezi, Y., and M. Van der Baan, 2015, Interferometric assessment of clamping quality of borehole geophones: GEOPHYSICS, **80**, WC89–WC98.

Van Sandt, D., and F. Levin, 1963, A study of cased and open holes for deep-hole seismic detection: GEOPHYSICS, **28**, 8–13.

Wapenaar, K., D. Draganov, R. Snieder, X. Campman, and A. Verdel, 2010, Tutorial on seismic interferometry: Part 1–basic principles and applications: GEOPHYSICS, **75**, 75A195–75A209.

Wuenschel, P. C., 1976, The vertical array in reflection seismology some experimental studies: GEOPHYSICS, **41**, 219–232.

Yaskevich, S., G. Loginov, A. Duchkov, I. Kerusov, and V. Vingalov, 2015, Reprocessing and quality control for microseismic data processing applications: Seismic technologies (in Russian), **3**, 48–54.

Zhang, Z., M. Nava, and J. Rector, 2016, Resonance in downhole microseismic data and its removal, *in* SEG Technical Program Expanded Abstracts 2016: Society of Exploration Geophysicists, 2652–2656.

LIST OF FIGURES

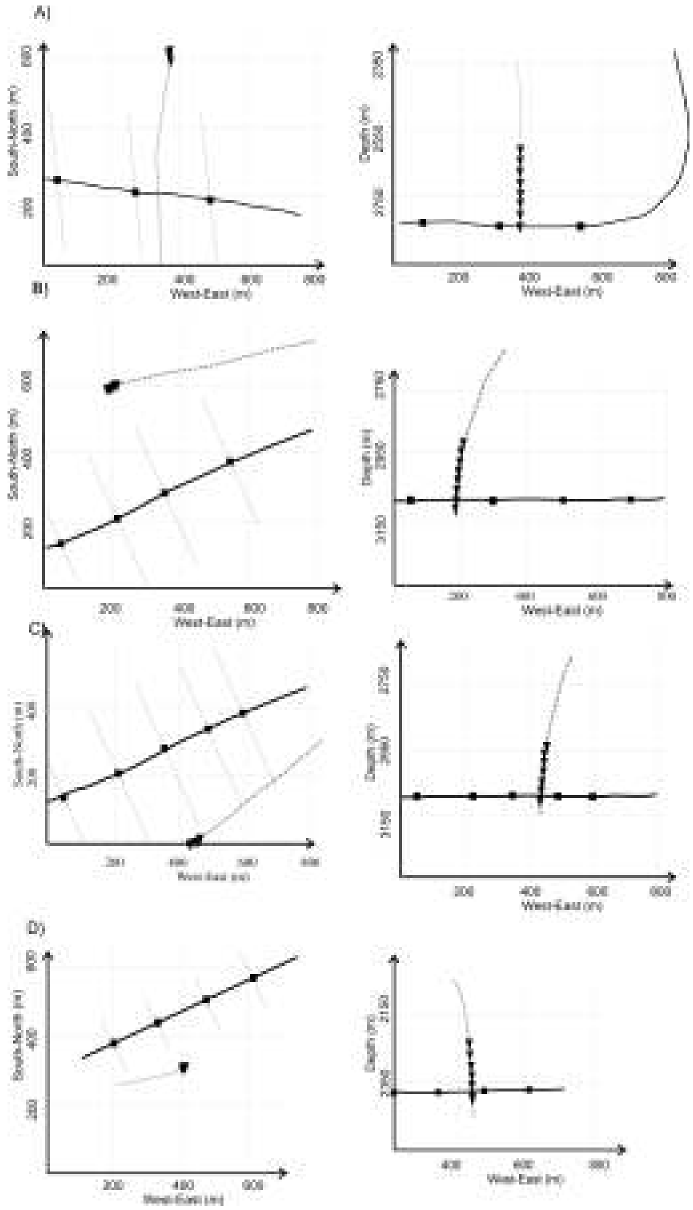

1. A schematic view of acquisition geometry for the monitoring datasets A, B, C, D. The plane view is on the left side, the EW view is on the right side. Black triangles show seismic receiver positions, dashed grey line shows monitoring well, squares - fracturing port positions with lines showing fracture direction and length

900x1581mm (600 x 600 DPI)

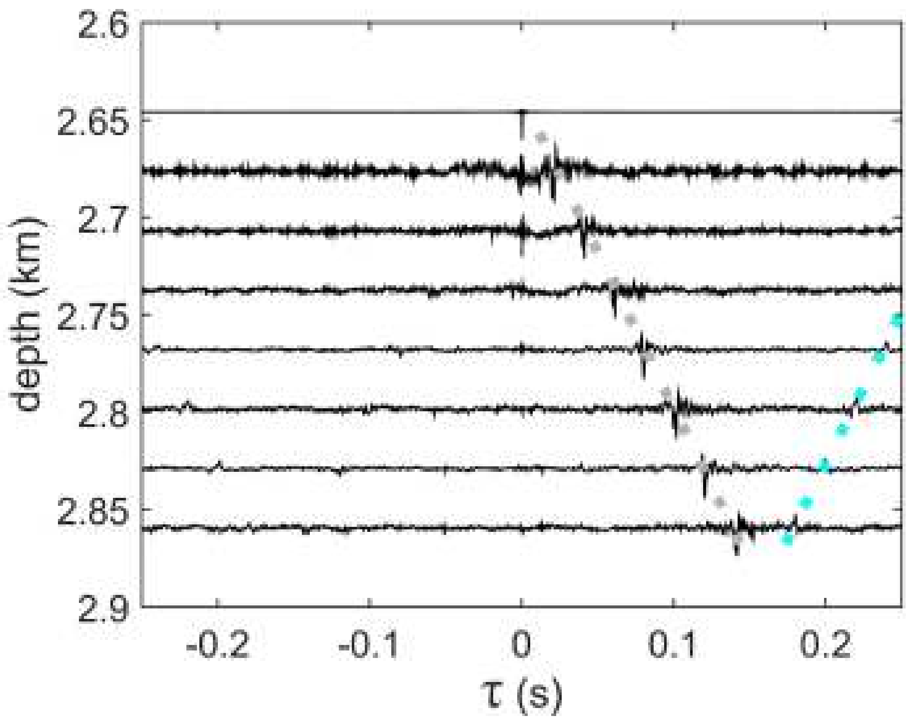

2a. Virtual-source gathers for the dataset A after band-pass filter: (a) [5-10-500-2000] Hz, (b) [5-10-30-60] Hz - 1st receiver as a virtual source; (c) [5-10-500-2000] Hz, (d) [5-10-30-60] Hz - 4th receiver as a virtual source. The dotted line shows 1.5 km/s apparent velocity (grey for the down-going and blue for up-going tube waves), dashed line - 3.5 km/s apparent velocity

148x111mm (300 x 300 DPI)

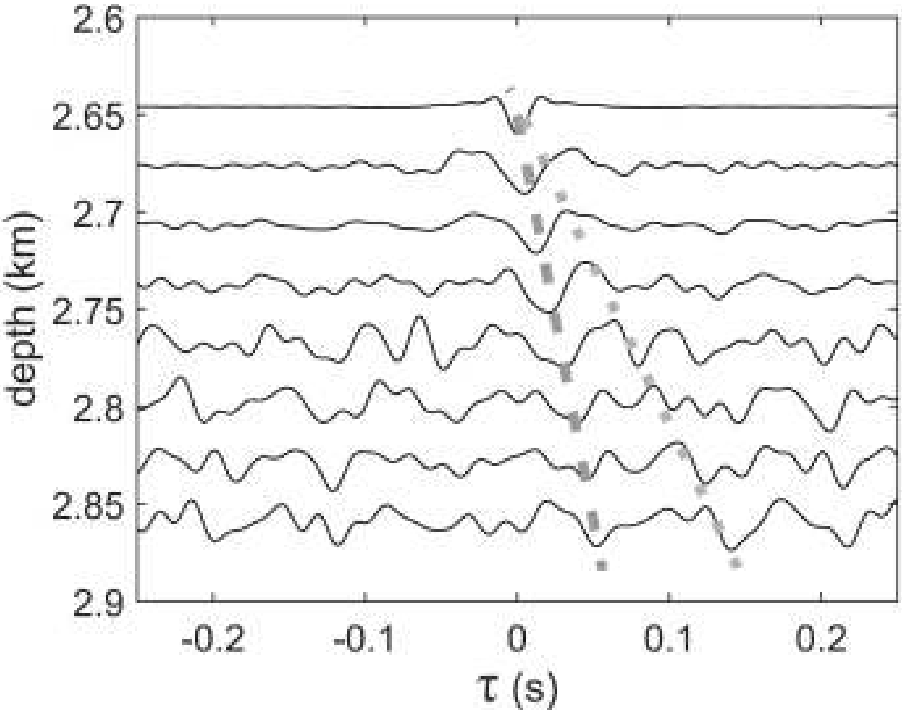

2b. Virtual-source gathers for the dataset A after band-pass filter: (a) [5-10-500-2000] Hz, (b) [5-10-30-60] Hz - 1st receiver as a virtual source; (c) [5-10-500-2000] Hz, (d) [5-10-30-60] Hz - 4th receiver as a virtual source. The dotted line shows 1.5 km/s apparent velocity (grey for the down-going and blue for up-going tube waves), dashed line - 3.5 km/s apparent velocity

148x111mm (300 x 300 DPI)

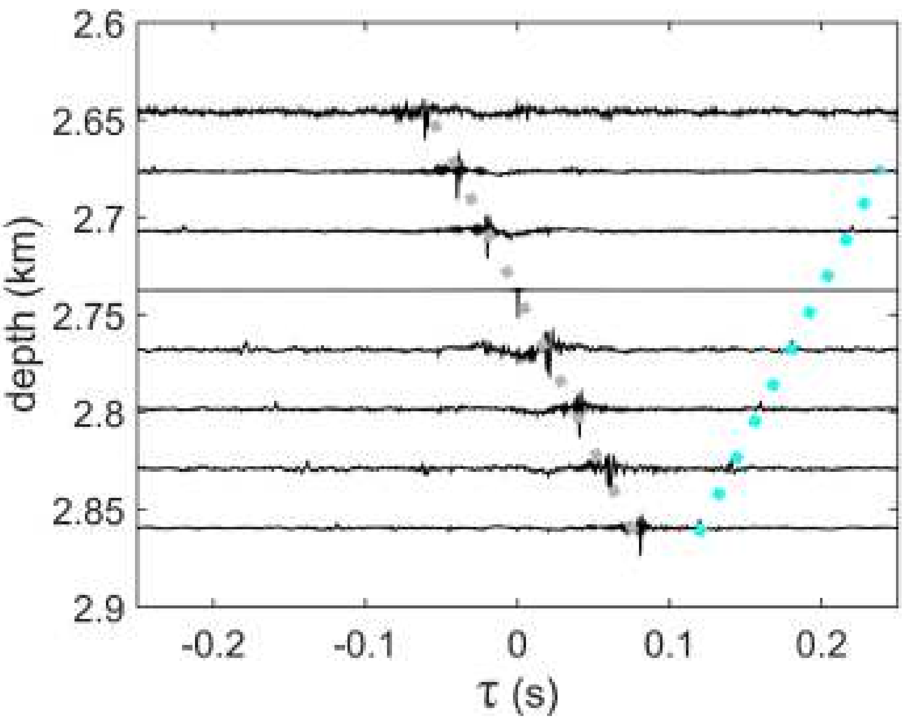

2c. Virtual-source gathers for the dataset A after band-pass filter: (a) [5-10-500-2000] Hz, (b) [5-10-30-60] Hz - 1st receiver as a virtual source; (c) [5-10-500-2000] Hz, (d) [5-10-30-60] Hz - 4th receiver as a virtual source. The dotted line shows 1.5 km/s apparent velocity (grey for the down-going and blue for up-going tube waves), dashed line - 3.5 km/s apparent velocity

148x111mm (300 x 300 DPI)

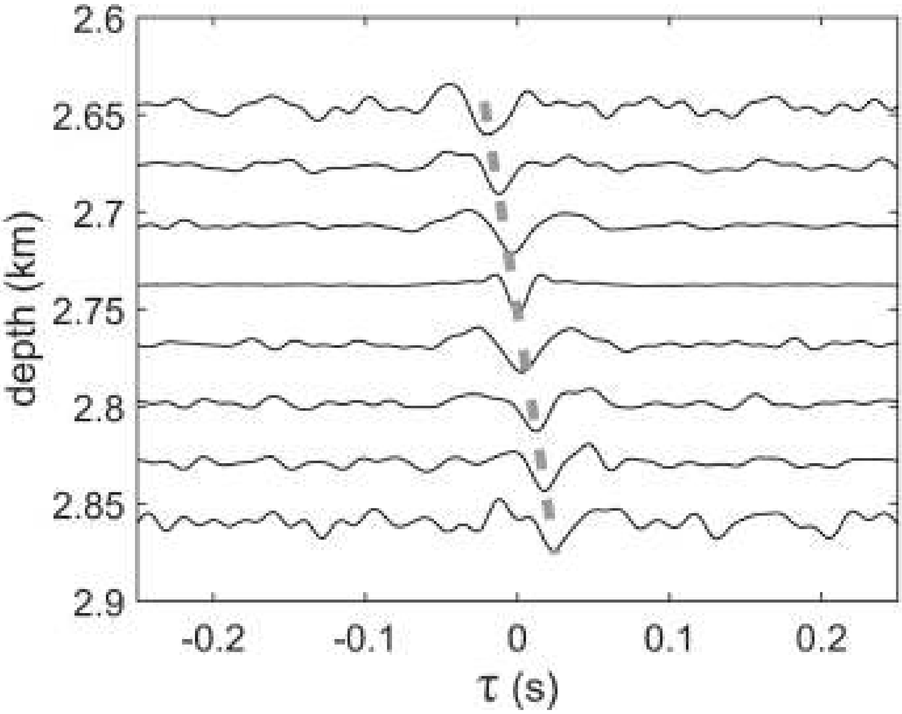

2d. Virtual-source gathers for the dataset A after band-pass filter: (a) [5-10-500-2000] Hz, (b) [5-10-30-60] Hz - 1st receiver as a virtual source; (c) [5-10-500-2000] Hz, (d) [5-10-30-60] Hz - 4th receiver as a virtual source. The dotted line shows 1.5 km/s apparent velocity (grey for the down-going and blue for up-going tube waves), dashed line - 3.5 km/s apparent velocity

148x111mm (300 x 300 DPI)

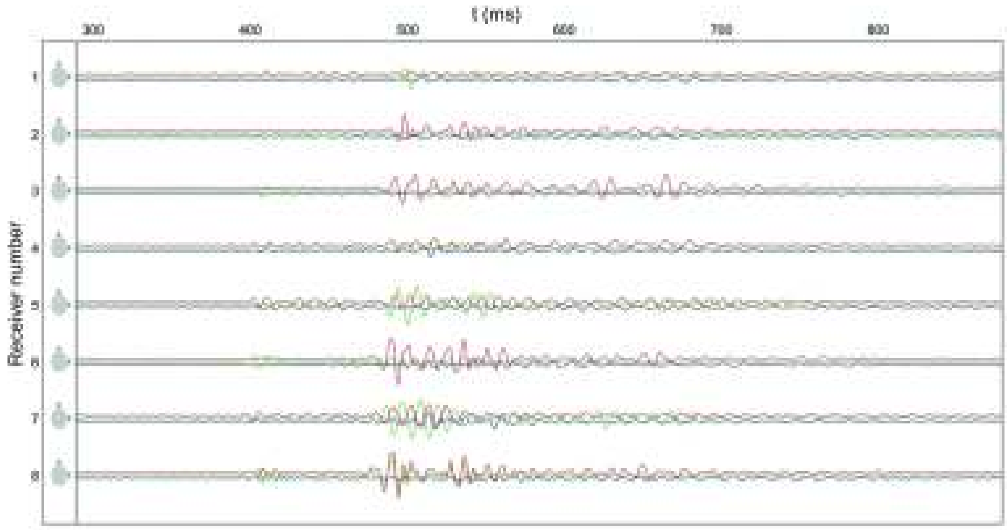

3. Microseismic event record (dataset A). Red, green, blue colours mean X, Y (horizontal) and Z components respectively

211x112mm (300 x 300 DPI)

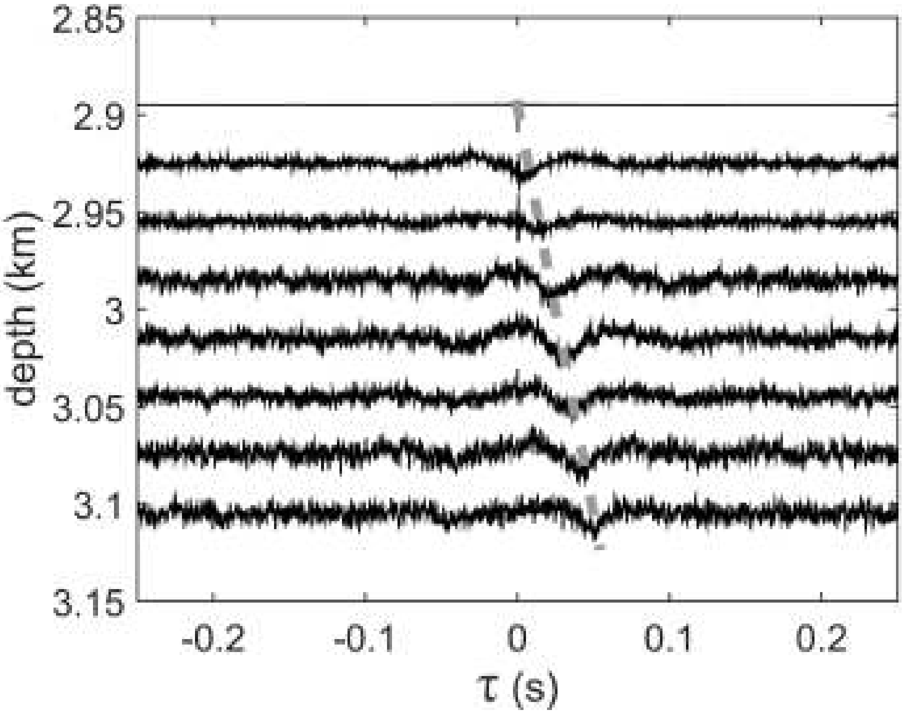

4a. Virtual-source gathers for the dataset B (1st receiver as a virtual source) filtered with band-pass filter: (a) [5-10-500-2000] Hz, (b) [5-10-30-60] Hz

148x111mm (300 x 300 DPI)

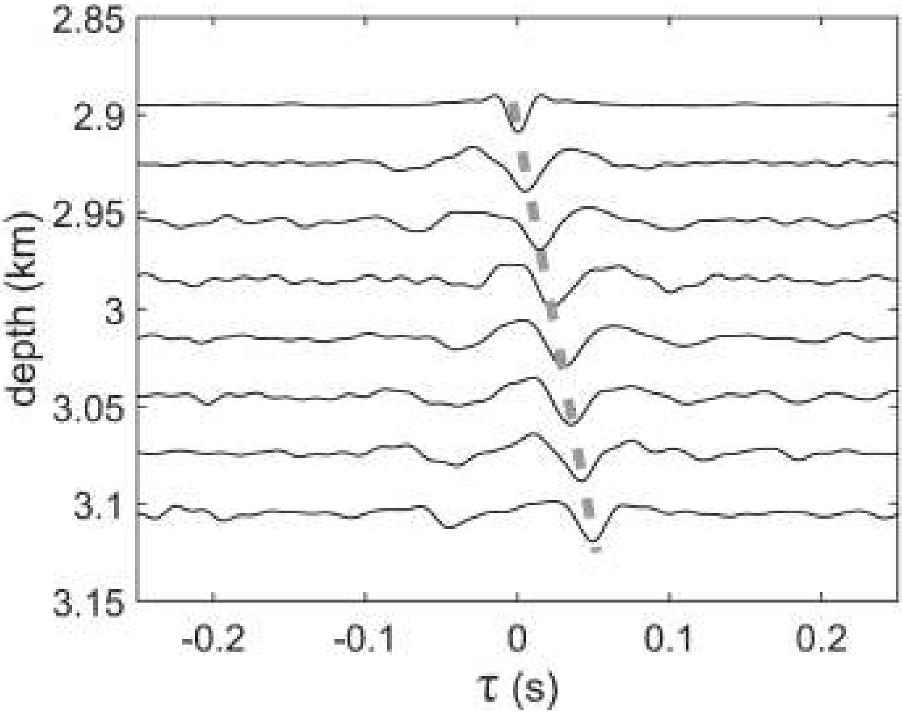

4b. Virtual-source gathers for the dataset B (1st receiver as a virtual source) filtered with band-pass filter: (a) [5-10-500-2000] Hz, (b) [5-10-30-60] Hz

148x111mm (300 x 300 DPI)

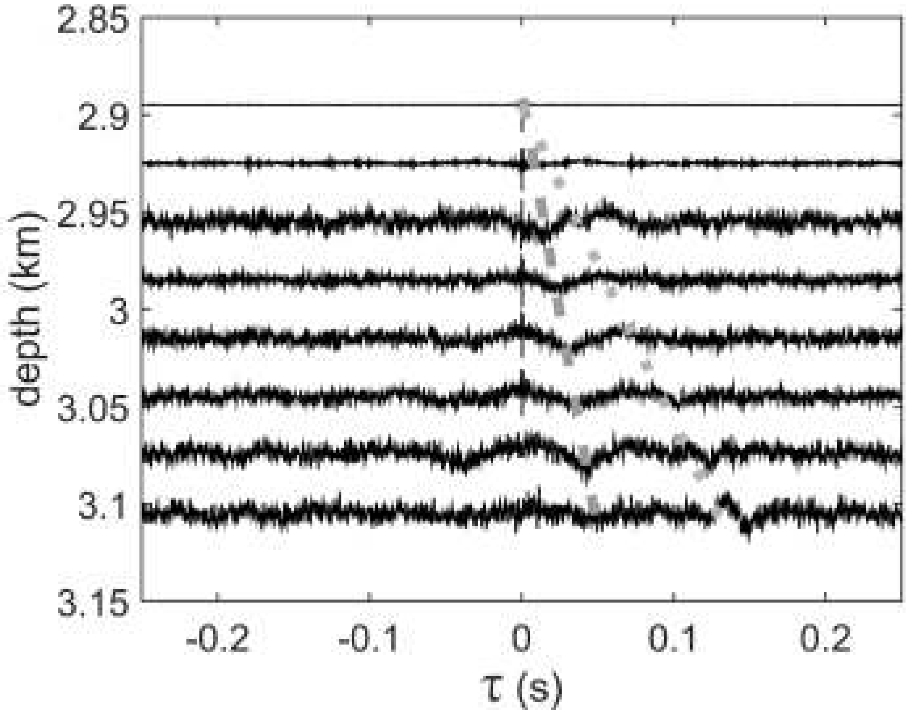

5a. Virtual-source gathers for the dataset C: (a, b) -- 1st receiver as a virtual source, (c, d) -- 8th receiver as a virtual source. Band-pass filter applied: (a) [5-10-500-2000] Hz, (b) [5-10-30-60] Hz, (c) [5-10-30-60] Hz, (d) [1-5-10-20] Hz. Dotted line -- 1.5 km/s apparent velocity (tube wave), dashed line -- 4.0 km/s apparent velocity (body wave)

148x111mm (300 x 300 DPI)

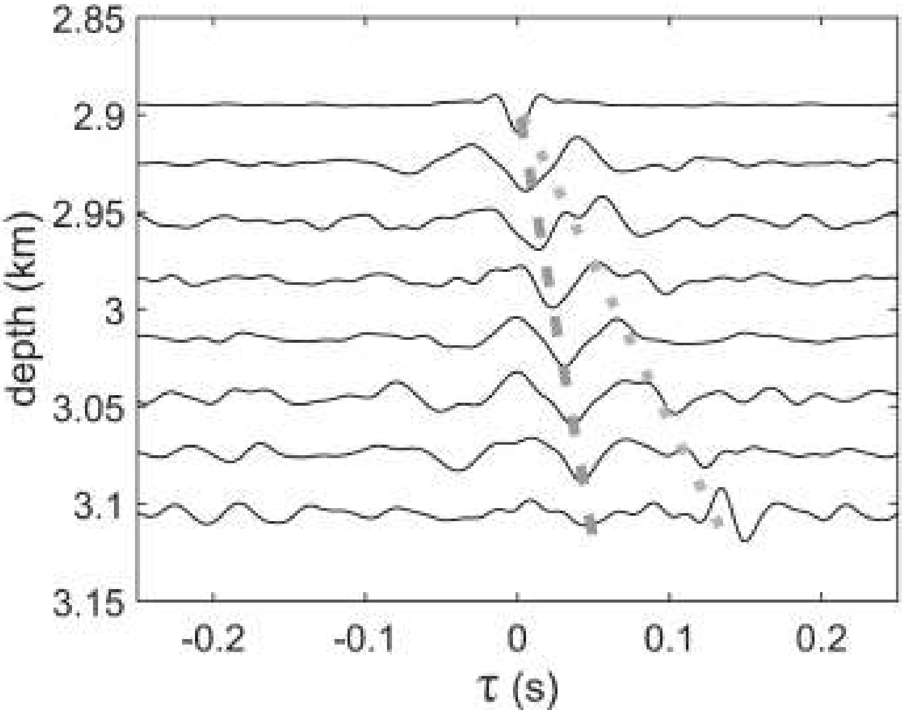

5b. Virtual-source gathers for the dataset C: (a, b) -- 1st receiver as a virtual source, (c, d) -- 8th receiver as a virtual source. Band-pass filter applied: (a) [5-10-500-2000] Hz, (b) [5-10-30-60] Hz, (c) [5-10-30-60] Hz, (d) [1-5-10-20] Hz. Dotted line -- 1.5 km/s apparent velocity (tube wave), dashed line -- 4.0 km/s apparent velocity (body wave)

148x111mm (300 x 300 DPI)

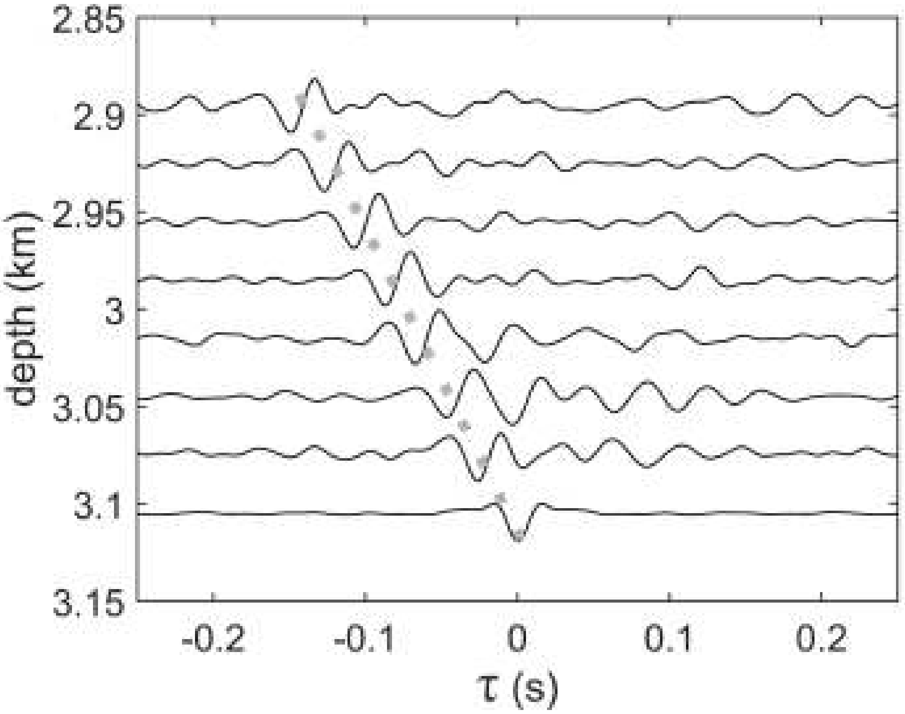

5c. Virtual-source gathers for the dataset C: (a, b) -- 1st receiver as a virtual source, (c, d) -- 8th receiver as a virtual source. Band-pass filter applied: (a) [5-10-500-2000] Hz, (b) [5-10-30-60] Hz, (c) [5-10-30-60] Hz, (d) [1-5-10-20] Hz. Dotted line -- 1.5 km/s apparent velocity (tube wave), dashed line -- 4.0 km/s apparent velocity (body wave)

148x111mm (300 x 300 DPI)

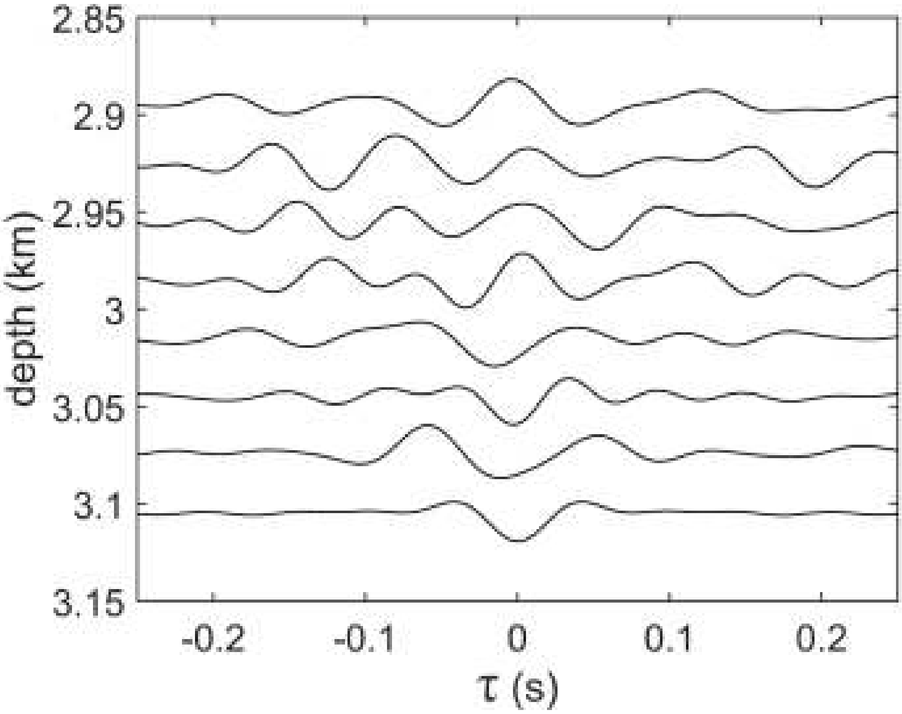

5d. Virtual-source gathers for the dataset C: (a, b) -- 1st receiver as a virtual source, (c, d) -- 8th receiver as a virtual source. Band-pass filter applied: (a) [5-10-500-2000] Hz, (b) [5-10-30-60] Hz, (c) [5-10-30-60] Hz, (d) [1-5-10-20] Hz. Dotted line -- 1.5 km/s apparent velocity (tube wave), dashed line -- 4.0 km/s apparent velocity (body wave)

148x111mm (300 x 300 DPI)

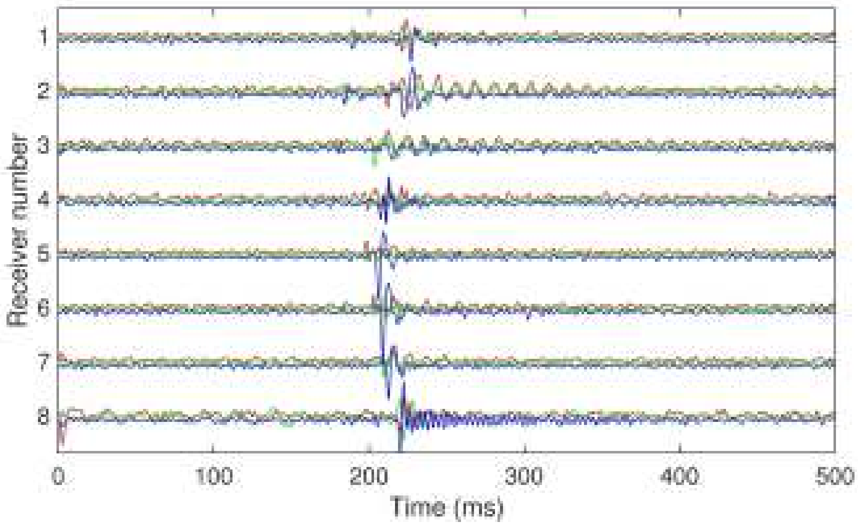

6. Microseismic event example (dataset C). Red, green, blue colours mean X, Y (horizontal) and Z components of the record respectively. So-called ``ringing'' is observed on the 8th receiver indicating problems with the receiver coupling

238x132mm (300 x 300 DPI)

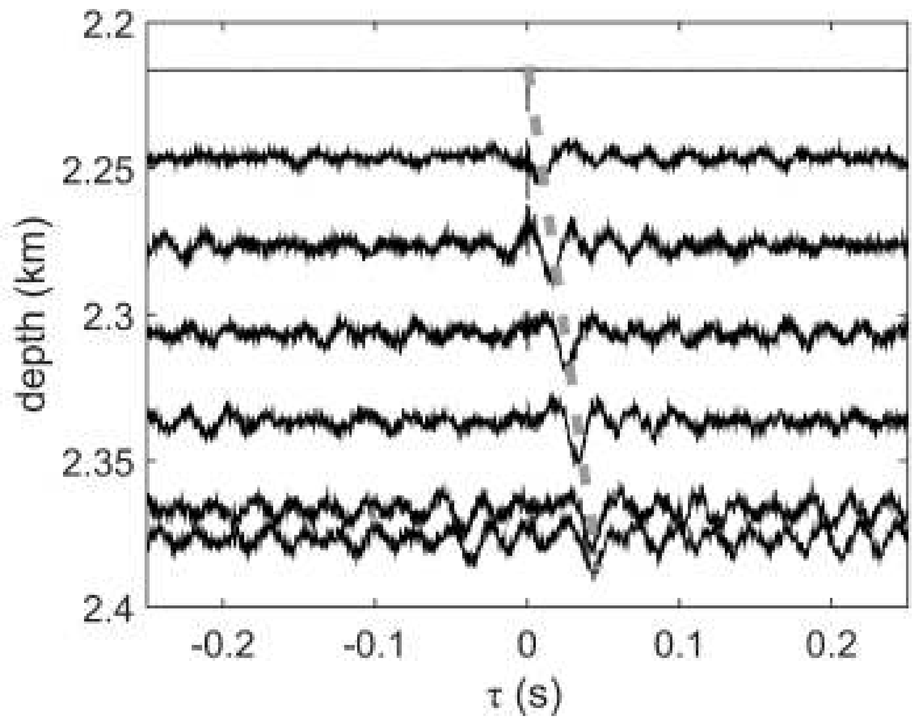

7a. Virtual-source gathers for dataset D (first receiver as a virtual source) after band-pass filter: (a) [5-10-500-2000] Hz, (b) [5-10-30-60] Hz. Dashed line -- 3.2 km/s apparent velocity

148x111mm (300 x 300 DPI)

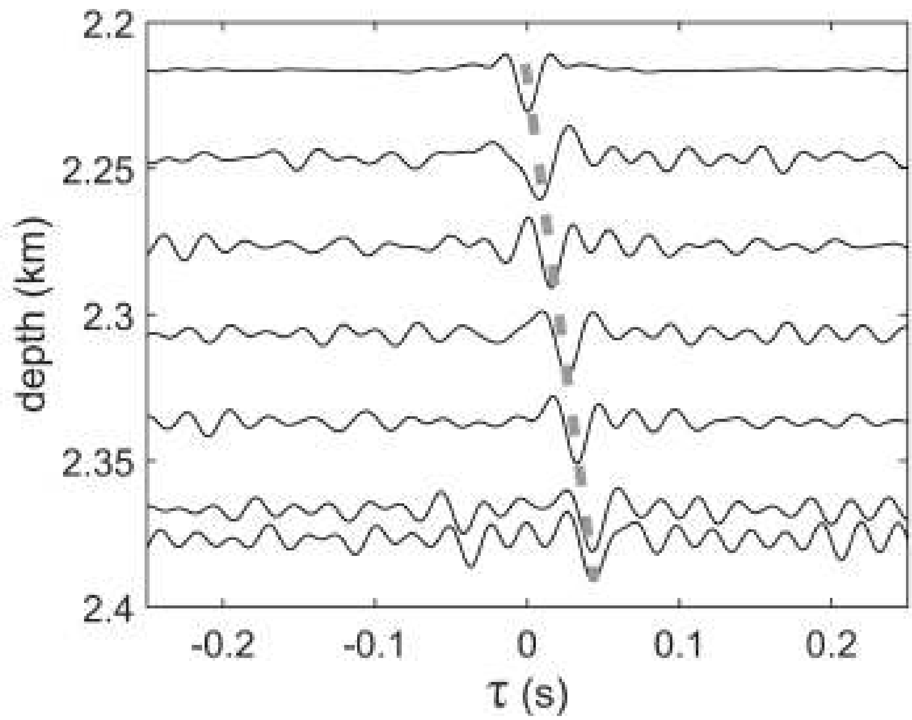

7b. Virtual-source gathers for dataset D (first receiver as a virtual source) after band-pass filter: (a) [5-10-500-2000] Hz, (b) [5-10-30-60] Hz. Dashed line -- 3.2 km/s apparent velocity

148x111mm (300 x 300 DPI)

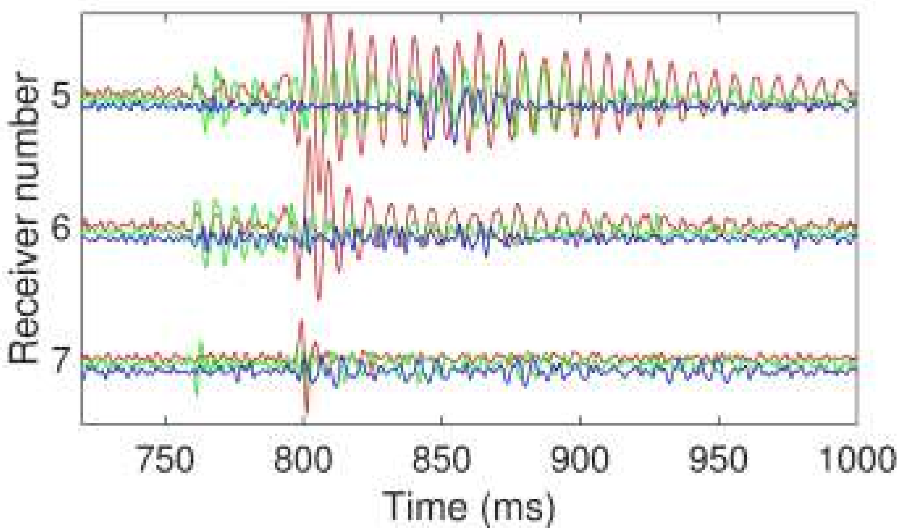

8. Microseismic event example (dataset D). Red, green, blue colours mean X, Y (horizontal) and Z components of the record respectively. Severe ``ringing'' is observed for horizontal components of receivers 5 and 6

197x110mm (300 x 300 DPI)

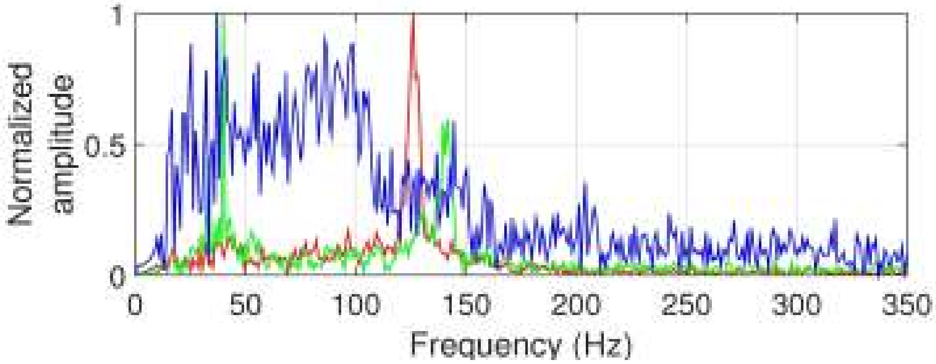

9. Amplitude spectra for one event (dataset D) recorded on the 5th receiver. Red, green, blue colours mean X, Y (horizontal) and Z components respectively

211x79mm (300 x 300 DPI)

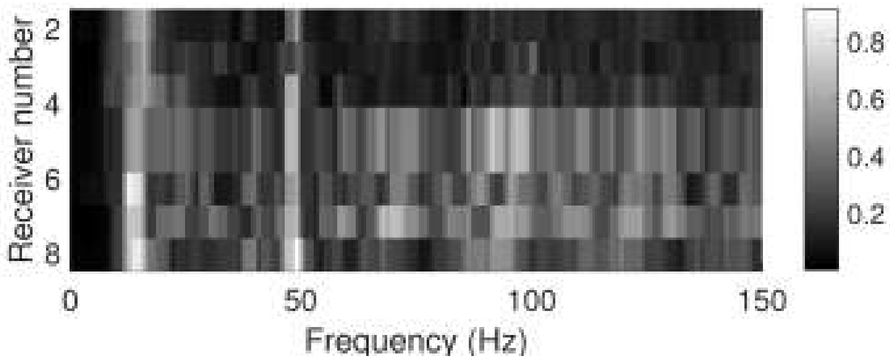

10a. Virtual-source gather normalized spectrum for datasets A, B, C, and D

211x79mm (300 x 300 DPI)

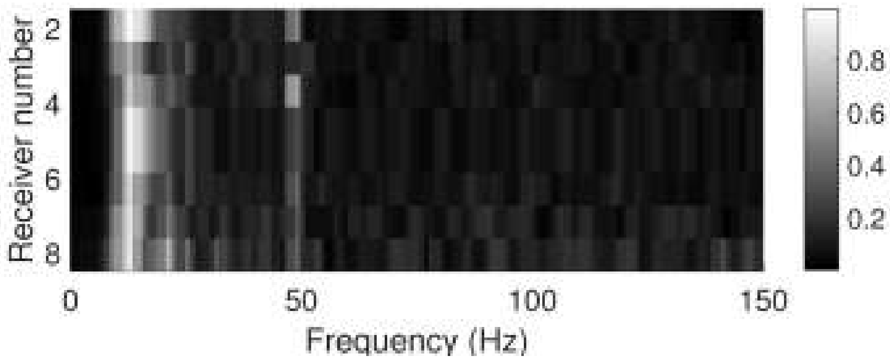

10b. Virtual-source gather normalized spectrum for datasets A, B, C, and D

211x79mm (300 x 300 DPI)

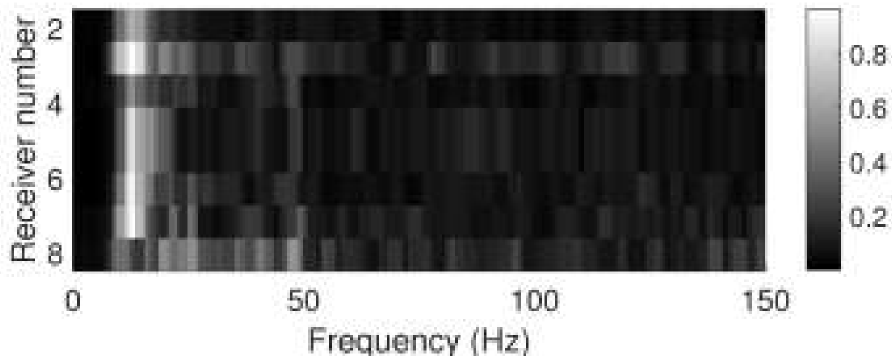

10c. Virtual-source gather normalized spectrum for datasets A, B, C, and D

211x79mm (300 x 300 DPI)

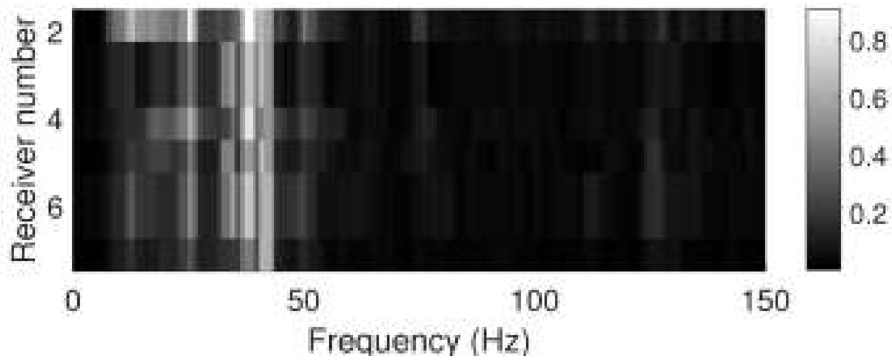

10d. Virtual-source gather normalized spectrum for datasets A, B, C, and D

211x79mm (300 x 300 DPI)

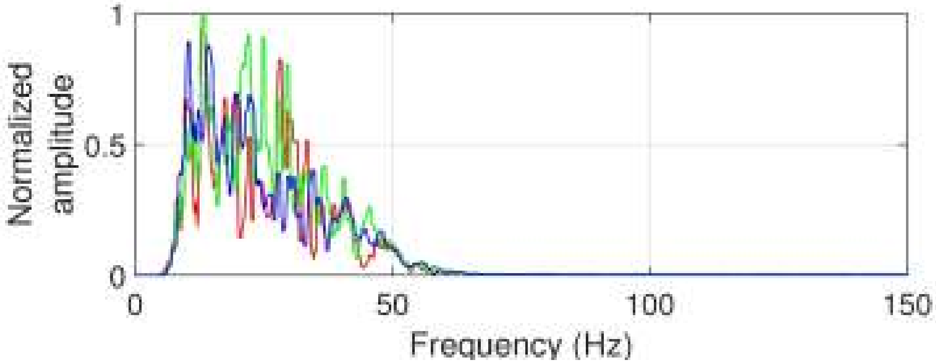

11a. Orientation-shot spectra for datasets A (8th receiver), B (8th receiver), C (8th receiver) and D (5th receiver); red, green, and blue colours stand for X, Y (horizontal), and Z components correspondingly

211x79mm (300 x 300 DPI)

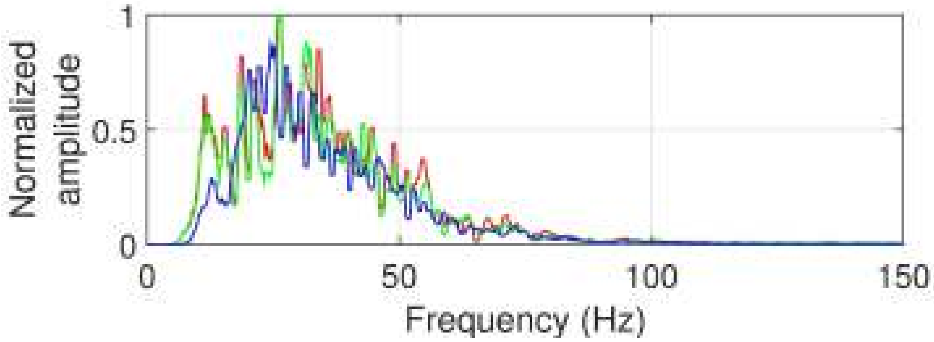

11b. Orientation-shot spectra for datasets A (8th receiver), B (8th receiver), C (8th receiver) and D (5th receiver); red, green, and blue colours stand for X, Y (horizontal), and Z components correspondingly

194x68mm (300 x 300 DPI)

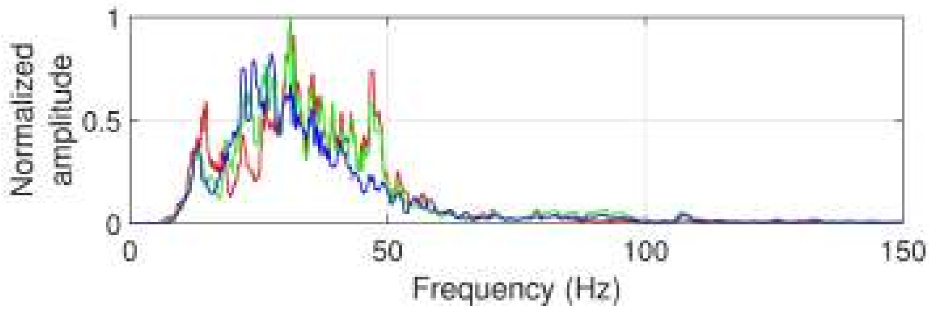

11c. Orientation-shot spectra for datasets A (8th receiver), B (8th receiver), C (8th receiver) and D (5th receiver); red, green, and blue colours stand for X, Y (horizontal), and Z components correspondingly

225x70mm (300 x 300 DPI)

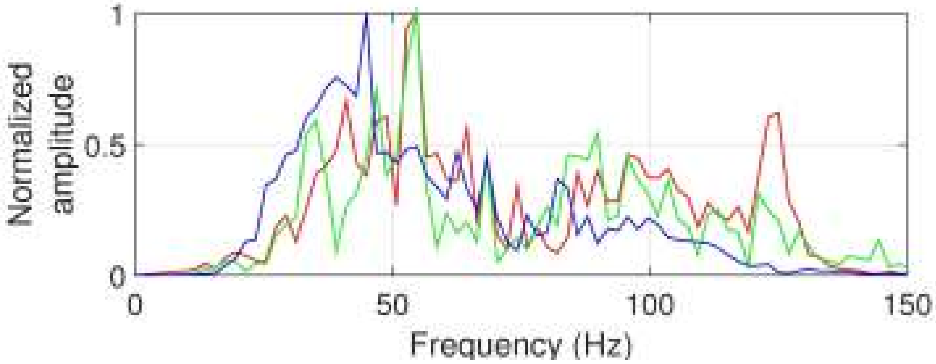

11d. Orientation-shot spectra for datasets A (8th receiver), B (8th receiver), C (8th receiver) and D (5th receiver); red, green, and blue colours stand for X, Y (horizontal), and Z components correspondingly

211x79mm (300 x 300 DPI)

Table 1 Summary on the applied seismic interferometry approach to the discussed datasets

Dataset	A	B, C (excl. 8th rec)	C 8th rec	D
Emergence frequency (Hz)	30	30	0	50
Dominant body-wave frequency (Hz)	25	25	0	45
Clamping quality from *emergence frequency*	moderate to poor	moderate	poor	good
Visible tube wave in a virtual-source gather	yes	no	yes	no
Visible clamping related resonances	no	no	yes (X,Y,Z rec.)	1-6 receivers (X,Y rec.)
Fluid level in the monitoring well (m)	0	-300 m	-300 m	-300 m
Tool diameter / Borehole diameter (mm)	48/110	48/110	48/110	48/110
Number of the recorded events	50	250	150	400

DATA AND MATERIALS AVAILABILITY

Data associated with this research are confidential and cannot be released.